Current Applied Science and Technology Vol. 22 No. 4 (July-August 2022)

Research article

Thermal Management for Green Vehicle Batteries under Natural and Forced Convection Modes

Jaya Jayabalan[1], Murali Govindarajan[2]*, Vajhala Venu Madhav[2] and Kannammal Jayabalan Sabareesaan[3]

[1]Department of Electronics and Communication Engineering, Hindusthan College of Engineering and Technology, Coimbatore, Tamil Nadu-6410150, India
[2]Department of Mechanical Engineering, Koneru Lakshmaiah Education Foundation, Vaddeswaram, Guntur District, Andhra Pradesh- 522 502, India
[3]Engineering Department,University of Technology and Applied Sciences, Nizwa, Sultanate of Oman

Received: 24 March 2021, Revised: 6 September 2021, Accepted: 2 October 2021

DOI: 10.55003/cast.2022.04.22.002

Keywords

air cooling;
Li-ion battery;
CFD;
BTMS;
film coefficient;
heat transfer coefficient

Abstract

The life span, efficiency and safety of lithium-ion batteries can be enhanced by temperature reduction and heat transfer optimization. The current research focuses on the cooling of lithium-ion batteries by reducing their temperature with optimized aluminum plates, which act like fins and carry away the heat due to convection in between the cells. For that, a seven cell battery pack model was built and cooling was done with air as a medium, which was manually passed through the system at a specified velocity using a blower. Considering the safety and cost as a key factors, dummy cells made of aluminum plates with heating coils inside were used rather than the original Li-ion battery for experimental studies. Numerical investigation of the temperature distribution on fins and the factors affecting the temperature reduction were performed. Free convection and forced convection methods were considered for the model using various calculated film coefficients. A reduction of 10ºC to 20ºC in temperature can be achieved using air which flows at a velocity of 8.5m/s. Numerical results are compared with the experimental results and the differences are discussed.

*Corresponding author: Tel.: +91 9442054281; Fax: +91 863 2388999
E-mail: muralinitt@gmail.com

1. Introduction

To eradicate the pollution issues, green vehicles can be alternatives to conventional automobiles. Furthermore, EV's are simple in construction, easy to operate, and create no emissions. Conventional automobile requires more oil resources, the combustion of which leads to pollution. Many researchers [1-4] have proposed new fuels and pollution control techniques to satisfy pollution control norms. Pang *et al*. [5] used R134a refrigerant in a DC air conditioning system run by a solar photovoltaic module to reduce the temperature rise inside the vehicle. The results showed that the DC air conditioning system improved environmental conditions inside the vehicle. Lu *et al*. [6] developed a 3D model staggered arrangement battery pack to calculate the effect of cooling and air supply. A resistance model of single irregular air passage was used. They concluded that when air was passed at the inlet and the outlet of the battery pack was at the top, better results were obtained. A new methodology was proposed and developed by Li *et al*. [7], who focused on reducing heat generation. The results showed that effective thermal performance could be achieved by optimization.

Two side wall battery modules were used to attain better heat dissipation, in which the cooling performance of a battery module at constant discharge rate of 6.94C (25A) kept fully open, was demonstrated [8]. A user defined function (UDF) was used at the time of simulation. It was found that high temperatures were reached in the middle of the battery pack. Kim *et al*. [9] discussed critical thermal issues and heat generation phenomenon associated with lithium-ion batteries. Therefore, maximum temperature and temperature difference between each BTMS is reviewed and proposed for effective solution of cooling. Chen *et al*. [10] designed a parallel air cooled BTMS using CFD methods in which both flow fields and temperature fields of the systems are calculated. It was noted that cell spacing decreased temperature but increased power consumption. To maintain power consumption, a plenum type was designed to improve the performance of BTMS. By adopting these strategies, the maximum temperature was decreased by 2.1 K compared to the original system. Deng *et al*. [11] summarized battery liquid cooling systems into three aspects, namely performance of coolant, classification of liquid cooling system, and battery pack design. They concluded that water cooling was more efficient than oil cooling and further addition of nano particles would give the best cooling performance. Patil *et al*. [12] studied the cooing performance characteristics of 20 Ah Lithium-ion pouch cells with cold plates along both sides by varying inlet coolant mass flow rate and temperature. The results indicated that with low inlet coolant mass flow rate and low inlet coolant temperature rate, a greater number of cold plate channels could increase cooling energy efficiency.

Chen *et al*. [13, 14] designed a cell spacing distribution of battery packs in parallel air-cooled BTMS for cooling efficiency improvement. The experimental air-cooled system with aluminum blocks was validated by the CFD method. The optimization of battery cell spacing was done by implementing optimization strategies. The results indicated that by implementing this strategy for optimization of battery cell spacing, the maximum temperature decreased by 4.0 K. Wang *et al*. [15] proposed power management strategies for reducing fuel consumption and battery degradation. Fuel cell degradation was studied using electrochemical models which gave analytical solutions for reducing fuel consumption and battery degradation. It was concluded that the degradation models included objective functions that could effectively enhance the lifetime of the fuel cell. A liquid to vapor cooling system was proposed for battery pack cooling [16]. Four different battery spacings were considered. It was observed that maintaining the battery spacing equal to twice the radius of the cells allowed maintenance of the coolant in liquid form. Therefore, the result showed that reducing space between batteries improved the thermal uniformity. Jiaqiang *et al*. [17] developed 60 battery cells to identify their thermal performance. By using the CFD method and lumped models of each cell, air cooling performance of the battery module was estimated. The best cooling performance was achieved by locating the inlet and outlet air flow ways on opposite sides. In addition, adding a baffle improved performance. Transient simulations were used to discuss the distribution of temperature in the module. Bai *et al.* [18] used PCM for cooling pouch lithium-ion battery. Battery modules having different battery thickness were designed. The space between adjacent batteries and thermal conductivity of PCM were studied along with its cooling performance. The results showed that temperature rise was reduced by increasing the space between adjacent batteries and the thermal conductivity of PCMs was improved. A two-dimensional numerical [19-21] model for a lid-driven cavity using five distinct nanofluids to enhance convective heat transfer efficiency for cooling electronic devices was designed. The heat transmission of the solid block using a hybrid nanofluid of aluminum oxide and silver particles was analyzed numerically, as well as the hybrid carbon nanofluid application in a rectangular micro channel. Based on the results, single wall carbon nano tubes may clearly be utilized in advanced cooling applications. In electric and hybrid electric cars [22], battery management and propulsion systems are critical. The results showed that only in the constant power area will the main acceleration be detected with a minimum power rating.

Panjagala *et al*. [23] successfully analyzed the aero heating processes under different spike geometrics by CFD. Finally, it was observed that employing a spike in the frontal region of the nose could reduce aero heating, and that CFD was a flexible model for examining heat production processes properly. ANSYS software [24] was used to do a heat transfer analysis on a car radiator by changing coolants with different volume percentages. In the battery pack for electric vehicles [25], a novel design has been proposed. Different coolant flow velocities at different discharge rates were used to test the battery pack's efficiency. The thermal efficiency was found to be better when the optimum temperature was less than 45ºC. On a spiral plate heat exchanger using hybrid nanofluids and nanofluids, a heat transfer analysis was performed [26]. When compared to water and nanofluids, the combination of hybrid nanofluids (Al_2O_3 + CuO/H_2O, Al_2O_3 + TiO_2/H_2O) showed better performance.

With the rise of electric cars [27], the most challenging part of the automobile industry is lithium-ion battery charging. To address these concerns, better charging stations, topologies of energy electronics converters, and other measures may be taken to improve battery life and performance. The thermal performance of trapezoidal cut twisted tape was studied using CFD at Reynolds numbers ranging from 2000 to 12000, and the findings were compared with plain tube using Fe_3O_4 nano fluid [28]. It was shown that the characteristics of circular tubes with a twist ratio of 4.0 produced better results and a higher heat transfer rate than plain tubes. On a tubular heat exchanger for turbulent flow with hybrid nanofluids (Al_2O_3-SiO_2/water and AlN-Al_2O_3/water) at multiple volume concentrations, a numerical simulation was carried out [29]. According to the final result, the heat transfer characteristics were determined at 0.2% Al_2O_3-1.8% SiO_2/water.

There are different types of cooling methods available to keep batteries within their optimal temperature, and we use a thermal management system relying on either air or liquid cooling. A similar kind of work was done experimentally. However, in order to avoid the bigger constraints, some of the components were neglected and the differences between experimental and simulation graphs were drawn in this paper. The real effects of temperature on battery cells during charging and discharging states, along with its effects due to environment and various operating conditions were also discussed.

2. Materials and Methods

2.1 Model description

Figure 1(a) shows that the dimensions of the single cell are 130 mm (width) x 206 mm (length) x 7 mm (thickness). A set of fins consists of one straight fin placed in between two bended fins, as shown in Figure 1(b). These fins are made of aluminium sheets with 130 mm (width) x 426 mm (length) x 0.5 mm (thickness). To prevent collision between the straight and bended fins, the bended fins have an angle of 2 degrees with straight fin, and the design of the straight fins between bended fins with the above discussed dimensions are created in CATIA, as shown in Figure 1(b). Therefore, all fins have extensions of 95 mm, which are mostly concerned with heat exchange with the surrounding environment.

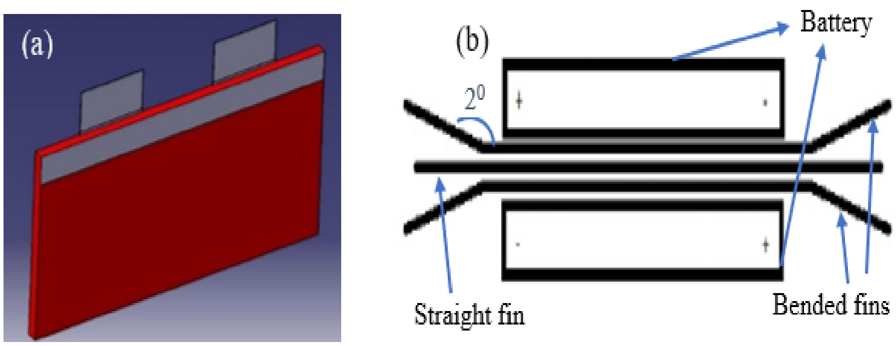

Figure 1. Li-ion cell design: (a) design of single cell, (b) fins placed in between cells

The bolt and nut M6 200 mm in length casing was designed with two square ports on the back side of the part to provide air flow in case of forced convection. These two open areas were designed in such a way to fix a blower with a funnel for the passage of air to carry away the heat generated on battery, as shown in Figure 2. Then, a set of seven Li-ion cells were placed between straight and bended fins. However, in the simulations, these complete parts like blower, holes on fins, and bolts and nuts were totally neglected in order to avoid bigger constraints. Figure 2 shows the complete model of the geometry, with all pars of the design assembled using CATIAV5.

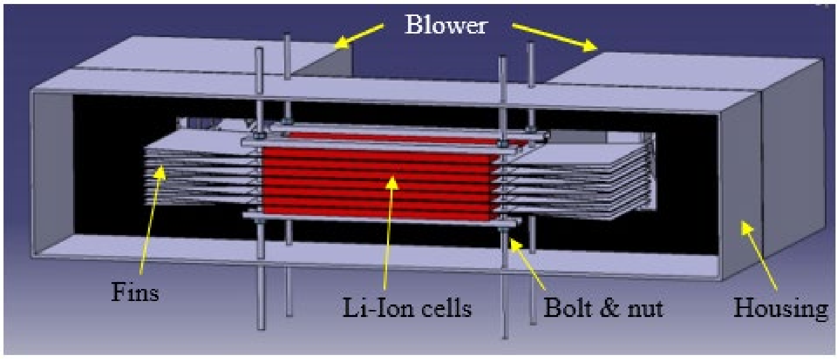

Figure 2. Assembled parts of Li-ion with fins

2.2 Method introduced to resolve the issue

In the present study, a new method of cooling system was introduced and the temperature was reduced. Here, the Li-ion cells were placed between aluminium sheets that act as fins to carry away the heat and were arranged in parallel. Aluminium is a very good conductor of heat and can be cooled or heated in short period of time. Therefore, fins made of aluminium were used in this investigation. When air was blown on both sides of the closed pack from one end continuously, heat generated between the cells was carried away by means of convection. Thereby, temperature is reduced. Figure 1(b) shows the concept being introduced in the current work.

This reduction in temperature and the effects due to air flow were studied by simulating the model using ANSYS software. Here, fluid flow CFX was carried out to study the effects of temperature at forced and free convection. This work was also performed experimentally using the original setup and the results were compared with simulations.

2.3 Fin optimization

Fin should be optimized to give a better performance. In order to achieve compatibility and effectiveness, fin geometry must be optimized. This optimization can be done by considering the various thermo physical properties listed in Table 1.

Table 1. Thermo physical properties

Parameters	Values
Ambient temperature (υ_u)	20°C
Cell temperature (υ_o)	60°C
Thermal conductivity of Al (λ_{Al})	237 W/m-K
Heat Transfer Coefficient by air (α_u)	5-25 W/m^{2}K

The effect of heat transfer on the fin depends on parameter m and length h of the fins while m is defined as a function of the fin's parameters and characteristics. The width of fins is equal to the width of lithium battery cell. This helps to distribute the total heat generated by the battery cells as it is transferred through the fin. The thickness of thin fins was taken as 0.5 mm.

To calculate length of fin (h), the parameter m is calculated as:

$$m = \sqrt{\frac{\alpha_U \cdot U}{\lambda \cdot A}}$$

where A = surface area, U = circumference of fin

Here in general, α_u = 10 W/m^{2}K and the temperature of the fin is expected to be 45°C. Therefore, the temperature differences between cells, fins and ambient environment are defined.

Figure 3 shows that graph between temperature difference of cells and length. The value 0.6 should be noted on the graph because there is a strong relationship between temperature difference and the length of the fin, and which parameter should be established as the main aim of thr optimization section.

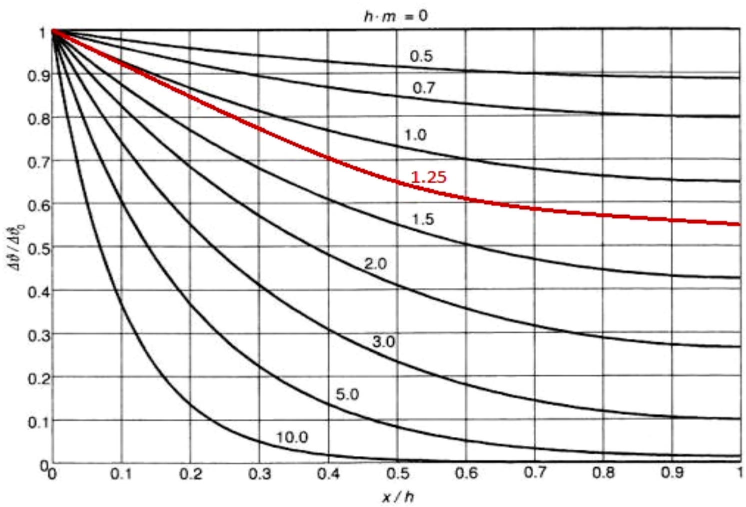

Figure 3. Fin optimization [13]

Line h . m = 1.25 was chosen due to the ratio of temperature difference. According to line characteristic, fins reach optimal temperature at the position of 60% of total fin length, and the optimal total length of the fin is calculated from the formula, $h = \frac{1.25}{m}$

So, from the above-mentioned result shown in Figure 2, it was confirmed that the length of the fin should start from 9.5 cm which was approximated as 10 cm. By considering the length of fin as 10 cm for this problem, there were also various other factors to be considered when installing the fin between the cells. The questions that arise were concerned with the number of fins to be installed in the system, the degrees by which bended fin should be placed, and the heat distribution over the fins. To arrive at a solution for these questions, a system was first started with a straight single fin between the cells, and then proceeded with a greater number of cells. Heat distribution over the fin depends upon the area of the fins. The greater the area, the larger the heat transfer would be. Bended fins are assumed to be placed on both sides of the straight fin. It can be bent at their ends by about 2 degrees. In addition, this supposed fin length proved optimal in free convection at normal room temperature. The effective cooling would be better in forced condition when a blower was attached to the system.

2.4 Simulation work

The simulation of the newly designed model at various times and temperatures, with respect to the film coefficient, was done in ANSYS. Here, the model was simulated to find the temperature change behavior of the system under free and forced convection. Simulation was carried out using ANSYS14.5 software. ANSYS was available in APDL (classic) and workbench version. For our work, the workbench methods were considered.

2.4.1 Methods to do simulation

The current work deals with reducing the temperature of battery pack by means of forced and free convection. There are various solver tools available in ANSYS for different types of simulation methods. Since temperature is the important parameter for this simulation, thermal solvers were dealt with. In order to solve the thermal behavior of battery issues, two solvers based on forced and free convections were considered. For free convection, transient thermal analysis was used as the solver. In this type of analysis, initial temperature and analysis settings are based on experimental methods. Other important parameters are film coefficient and ambient temperature. Film coefficient is the main parameter that determines the heat transfer rate from the body to the environment. These film coefficients are calculated as shown in Figure 3. After assigning the geometry on which the convection takes place, the solver calculates the varying results of temperature.

2.4.2 Calculation of film coefficient for free convection

Film coefficients were calculated from the equation shown below Table 2, and the calculation of film coefficient was done on excel sheet. It was calculated as convective film coefficient, at 45ºC, h = 4.02 W/m^{2}K. This film coefficient was applied to the overall free convection simulation methods at various temperatures with various film coefficients. Normal air parameters were considered to calculate the film coefficient. From the values of available initial temperature, battery temperature, fluid density and other parameters that were given on the excel sheet, the film coefficient was calculated. Table 2 shows the film coefficient calculation at 46ºC initial temperature. Similarly, for 67ºC and 77ºC, various film coefficients were calculated and applied to find the convection area and the heat transfer. Because of change in film temperatures, the film coefficient also changed, at 67ºC, h = 4.85 W/m^{2}K, and at 77ºC, h = 5.15 W/m^{2}K.

2.4.3 Calculation of film coefficient for forced convection

For forced convection, the film coefficient was not calculated using any of the above mentioned methods or equations. Here, the second solver was used to find the convective film coefficient. The second simulation solver used was Fluid Flow (CFX). This method was not used to calculate the complete thermal distribution but to find the film coefficient which was then again coupled with transient thermal analysis to find the temperature reduction. A steady state fluid flow CFX simulation was carried out by selecting all the parameters at initial conditions and then assigning the domains and boundary conditions. Solver CFX that was being used here for the simulation helped to create a fine mesh for more accurate gradient. Table 2 shows the property values for calculation of film cofficient.

Table 2. Property values considered for calculation for film coefficient

Properties	Values
Film temperature (T_f)	33ºC
Fluid density (ρ)	1.205 kg/m^3
Height of surface (L)	1.3 m
Fluid viscosity (μ)	1.98E-05 N-s/m^2
Fluid thermal conductivity (k)	0.0257 W/m-K
Fluid specific heat capacity (Cp)	1000 J/kg-K
Fluid thermal expansion coefficient (β)	0.003411 /K
Grashoff number (Gr)	7.08E+09
Rayleigh number (Ra)	5.05E+09
Prandtl number (Pr)	0.71

Correlation 1 (for all values of Ra) Nu = 204, h = 4.02 W/m^{2}K

$$\mathrm{Nu} = \left\{0.825 + \frac{0.387\mathrm{Ra}^{16}}{[1 + (0.492/\mathrm{Pr})^{9/16}]^{827}}\right\}^2$$

Correlation 2 (for all values of Ra) Nu = 138, h = 2.72 W/m^{2}K

$$(Ra \leq 10^9)$$

$$\mathrm{Nu} = 0.68 + \frac{0.670\mathrm{Ra}^{1/4}}{[1 + (0.492/\mathrm{Pr})^{9/6}]^{49}}$$

Calculation of inlet velocity

This velocity calculation was used to give the inlet values for forced convection. There are two inlets on the back side of the casing. In case of blower, its air flow velocity was taken into account.

Equation to calculate RPM to velocity:
V = C * rpm = Pi * D * rpm
Where, V = Velocity of air flow
C = Circumference of blower
D = Diameter of blower = 0.12 m
RPM = Rotations per minute = 1350 RPM
Pi = 3.14
By calculating, V = 3.14*0.12*1350
V = 508.68 m/min
To get m/s: V = 508.68/60 = 8.478m/s
Therefore, the velocity of air flowing through the funnel is 8.5 m/s (approx.)

2.4.4 Fluid flow CFX simulation

As already discussed, fluid flow CFX was used to calculate only the convective film coefficient. The required battery geometry was modeled and imported from CATIA, but the model was redesigned for solid and fluid domains. Here, the geometry had three parts: fluid, battery pack and housing. The battery pack was the solid domain, and the area where the fluid flows were completely assumed and modeled as the fluid domain. The solid domain was the original available part on which temperature distribution or reduction took place. This was already designed in CATIAV5. The fluid domain was an imaginary part which was created to give boundary conditions and produce closed parts.

The geometry for creating the fluid domain was completely assumed based on its inlet and opening boundary condition outlets. This domain was not valid in transient thermal analysis once the CFX was coupled to it. The housing was the third part which was taken into consideration for the simulation but it was not an imaginary one. It was an original part which was identical to that shown in Figure 4. Housing also helped to fixing boundary conditions. The main inlet boundary conditions were assumed based on housing geometry. The complete geometry used in fluid flow CFX is shown in Figure 5.

After assigning the geometry for the solver, the next step was to design an accurate and efficient meshing. If the complete system uses mesh elements that are too fine, there will obviously be a great number of nodes and elements, and the solver will need a lot of time to calculate. Firstly,

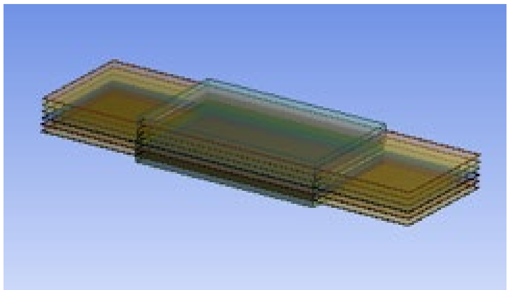

Figure 4. Solid domain

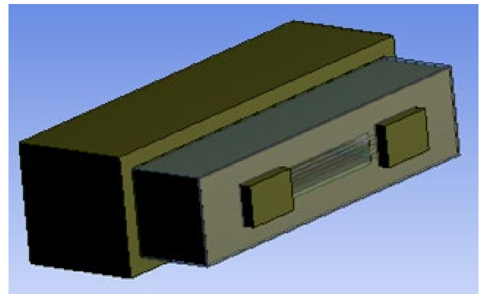

Figure 5. Complete CFX model

general mesh was applied to the system, and because it was very coarse, it affected the accuracy of the result. Therefore, a prism meshing was carried out here. It was mainly gradient and inflation that were related to meshing. So, the area to be analyzed was given a fine mesh and the other areas were given a medium size meshing. Meshing of the complete model is shown in Figure 6.

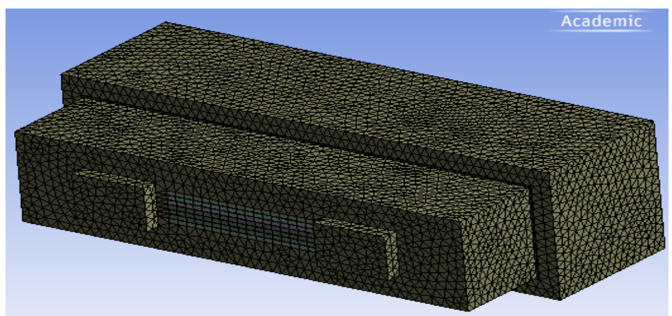

Figure 6. Mesh on model

For the solid domain, heat input in form of electricity was given as a boundary condition. For the fluid domain, two inlets were selected and an input value of velocity of 8.5m/s was given. For the outlet, an opening boundary condition was selected. After assigning the boundary conditions, the interface between fluid and solid domain had to be determined. Here, fluid- solid interface and solid-solid interface were assigned.

After meshing, it was noticed that the number of nodes = 38593 and number of elements = 157754 were very high. If the system has a greater number of elements, then the simulation will take a lot of time to complete. Therefore, on running the simulation, it was found that it took a greater number of iterations = 1575 to solve the problem. So, normal general meshing was chosen. The mesh had to be resized or the geometry changed to reduce the number of iterations and solution time. Reducing the mesh affected the accuracy of the result, so the geometry taken for observations was reduced. The model was symmetrical in both horizontal and vertical planes. Therefore, one fourth of the model was taken into observation. Then, the number of elements was obviously reduced. All parameters and data used for this geometry were the same as given in the full model. But here, there was only one inlet. Therefore, the other inlet parameters were suppressed. Also, prism meshing was done to increase the fineness of the mesh in order to increase the accuracy of results. Figure 7 shows the geometry of the new model.

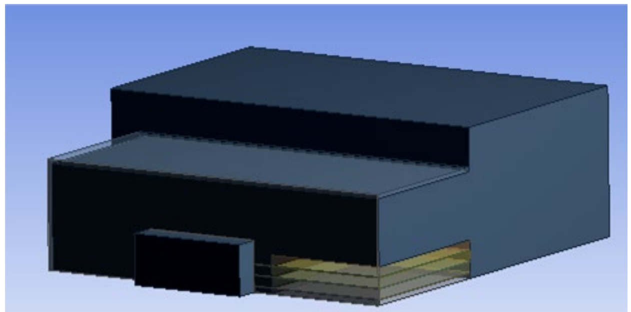

Figure 7. Model symmetry

In Figure 8(a), the mesh imposed on the model is shown in full. The heat transfer that takes place completely depends on the fins placed between the cells. So, mesh on fin parts needed to be finer to get accurate results. A particular area in Figure 8(b) was crowded with a greater number of elements because the fine mesh assigned to the fin parts used inflation in the solver. After giving the optimum meshing, the model was subjected to a boundary condition. Here, there is one inlet whose value is given as velocity of 8.5m/s.

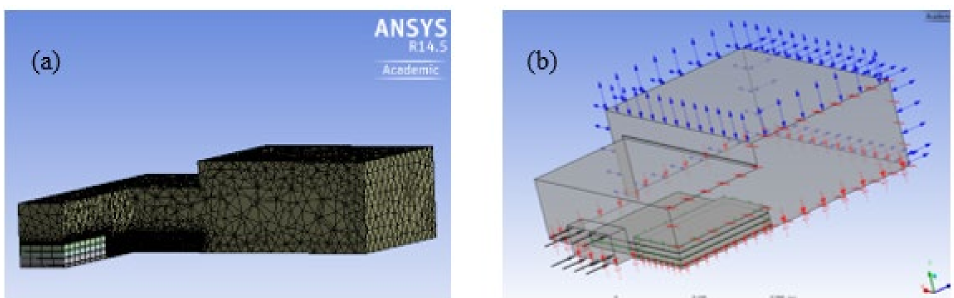

Figure 8. Symmetry model (a) Complete mesh on fins, (b) Boundary condition on symmetry model

After assigning values, the interfaces solver was determined for this simulation. Here, the overall conservation target was given as 0.01. Once all the input parameters were given, the setup was run for the simulation. The value of heat transfer film coefficient was obtained from the domain fluid solid interface 1. Figure 9 shows the calculated film coefficient. This value was mapped into transient thermal analysis to find the change in temperature under forced convection. In order to check whether the simulated heat transfer coefficient was accurate or not, the Y-plus value needed to be within a value of 1.

2.4.5 Y-plus calculation

Y plus is a dimensionless wall distance. It is used in boundary layer theory for defining the laws of the wall. This parameter helps to check the accuracy of the simulated value. The value of y plus should be 1 for the optimum mesh nodes. Figure 10 shows the Y plus value for the simulated normal mesh nodes. It is shown that the value of y plus was greater than 1. This error may have been due to

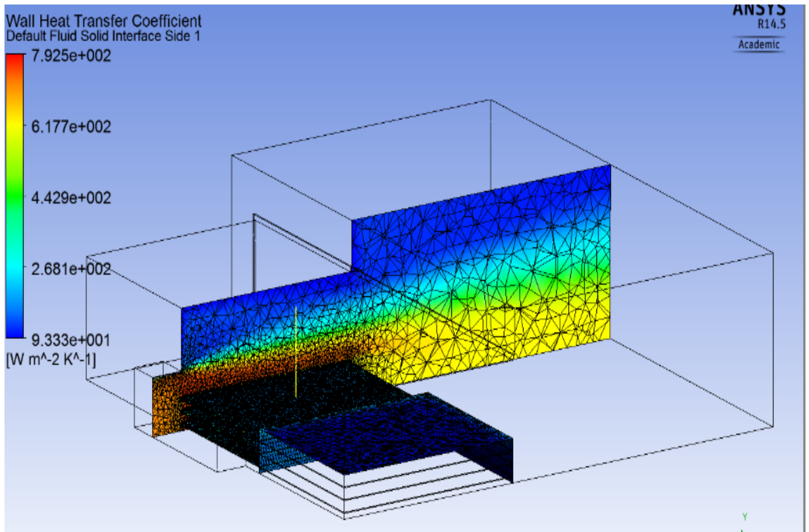

Figure 9. Heat transfer coefficient- non-optimized mesh

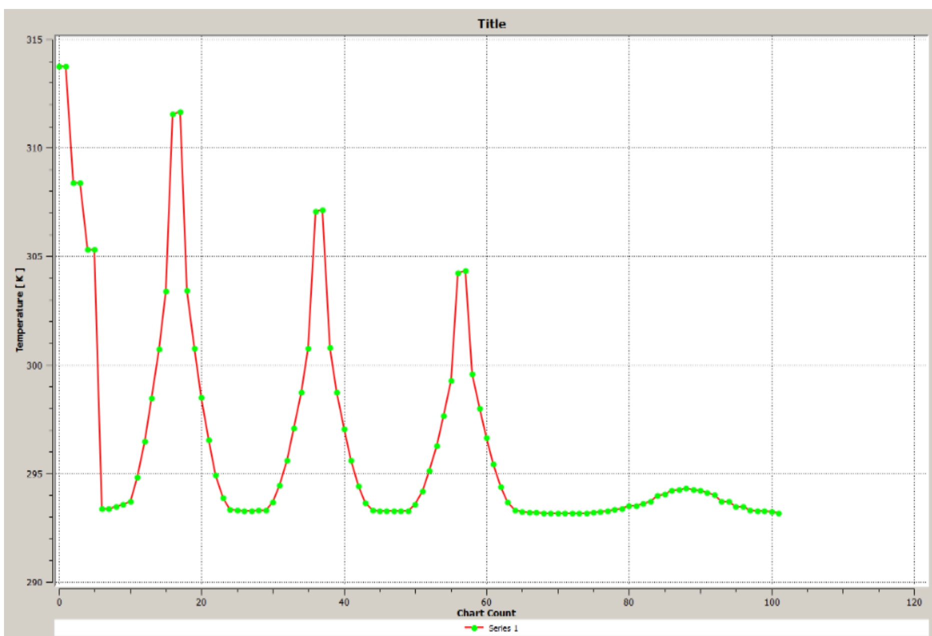

Figure 10. Y plus value for 7 layers

discretization error and model error. In order to reduce the error mesh independency study, further study had to be carried out.

When the results depend on nodes, the grid independent results need to be found. That is, mesh independency study should be done by varying the values of layers and aspect ratio, enabling average film coefficient to be found. This approach described and concluded that solving with these many nodes and mesh is not a difficulty with mesh dependency. In this study, the available simulation results had 224067 nodes in total, and this included both solid and fluid domains.

From Table 3, according to the independent mesh study, the value of film coefficient increased with greater difference but the value of temperature remained almost constant. It was therefore decided to find the optimum mesh by solving the temperature boundary layer. Figure 10 shows the Y plus value for 7 layers, and a graph that shows mesh node versus film coefficient is shown in Figure 11.

From Figure 10, it can be seen that the value of y plus ranges up to 7. So, to reduce the value of Y plus, a mesh independency study was carried out and the results shown in Figure 11 indicate that it does not reach a steady state. Therefore, Figure 12 was constructed to show the result of temperature boundary layer.

From Figure 13, there are only 8 nodes in a single layer. For an optimum mesh to be obtained, it has been recommended that a minimum of 10 nodes are required. Also, in this graph the lower portion shows the fluid region and the upper portion shows the solid part of the battery body. These node calculations are mainly for meshing. As a next step, we then checked the temperature boundary layer values for a greater number of aspect ratios. Figure 14 shows the number of nodes for 14 layers with 36 aspect ratios.

So, it is clearly seen that the number of nodes available in this series was greater compared to the recommended number of nodes. There were 12 nodes mentioned in Figure 14, which gave an optimized mesh value for the system. The Y Plus value for this process is shown in Figure 15. In addition, it is clear that the value of Y plus decreases to 5 from the value of 7. Since variation of the value of Y plus 5 did not cause a big error for the optimum range, these parameters were finally selected as being the best values to solve the issue. The film coefficient that was resolved using this criterion was taken as the calculated value to find the forced convection.

Therefore, the film coefficient calculated for the optimum mesh, which was an average calculated as $h_{avg} = 484.48$ W/m^{2}K. This heat transfer coefficient was then mapped into the transient thermal analysis solver in order to find the reduction in temperature under forced convection. Figure 16 shows the variation of film coefficient in the body. This variation is due to the velocity and air flow through the system.

Table 3. Independent mesh study

Layer	Aspect Ratio	Average Film Coefficient (W/m^2 K)	Nodes	Temperature (K)
7	12	185.445	224067	315.2
10	24	327.292	298656	316.29
14	36	484.48	367692	316.86
16	48	643.36	445268	316.87

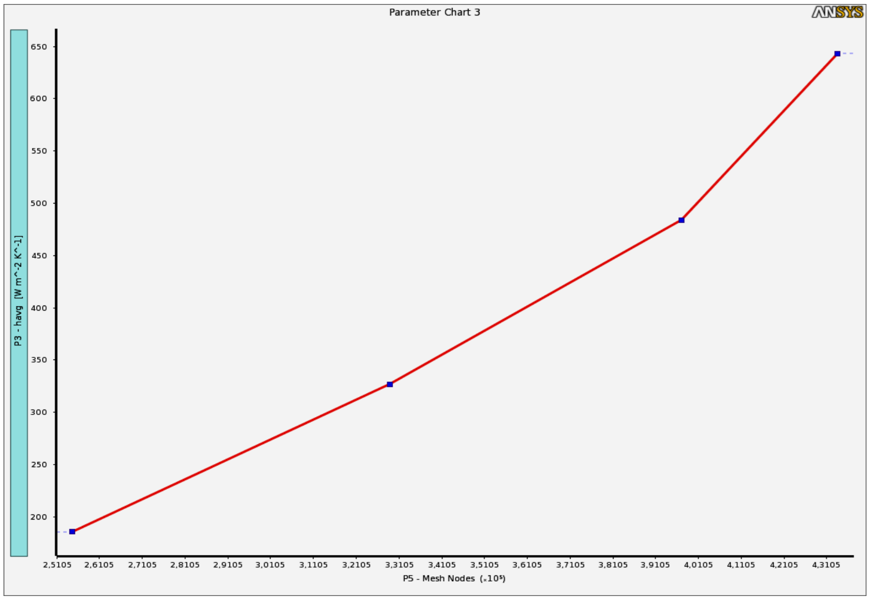

Figure 11. Mesh independency study, film coefficient vs mesh nodes

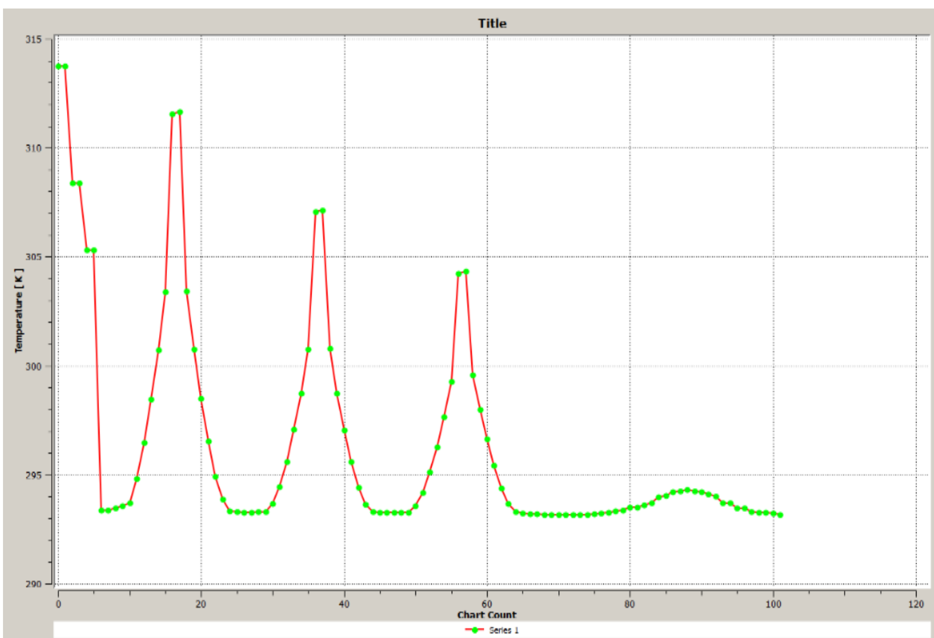

Figure 12. Temperature boundary layer for 7 layers

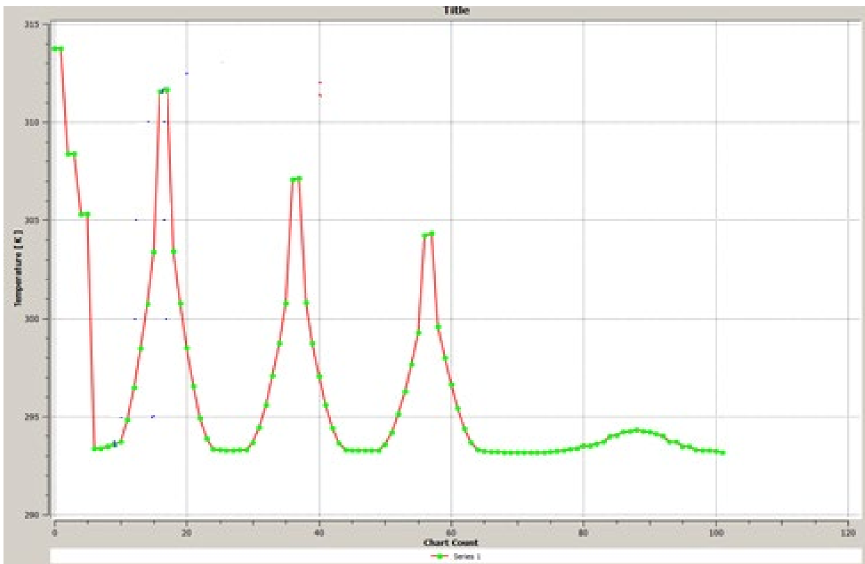

Figure 13. A layer with 8 nodes

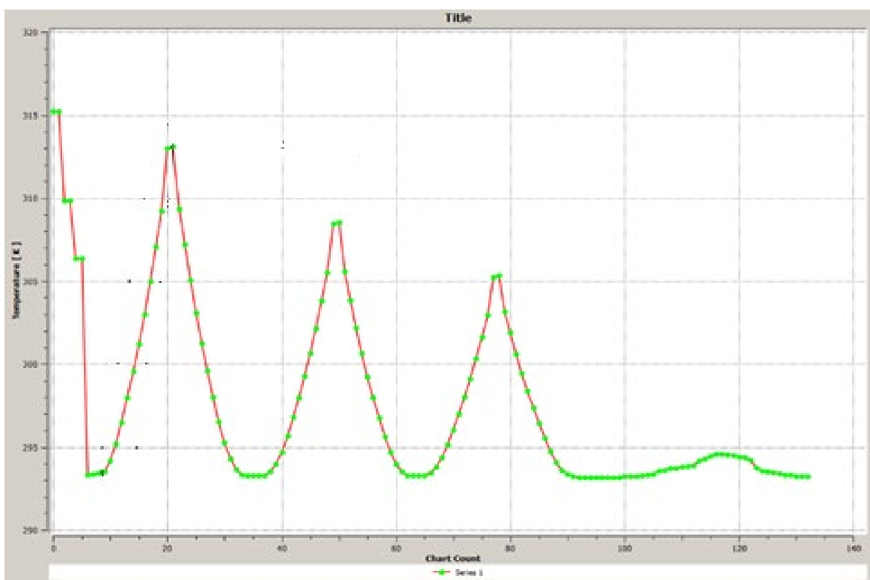

Figure 14. Temperature boundary layer for 12 layers with 12 nodes

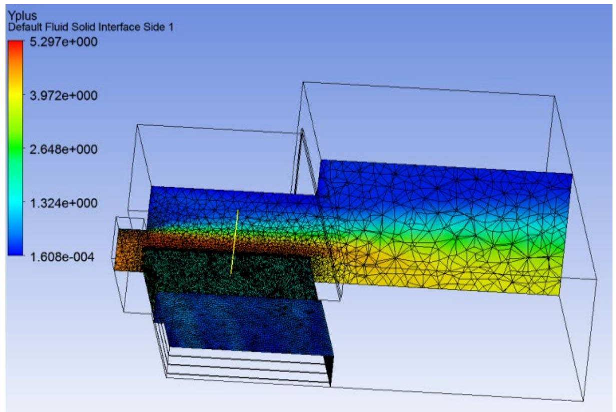

Figure 15. Y plus value for 12 layers

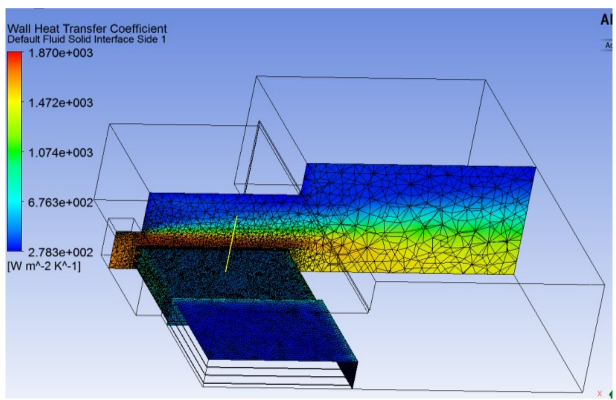

Figure 16. Heat transfer coefficient for optimized mesh

3. Results and Discussion

The simulation results were compared with the experimental results and the differences were discussed. Experimental results were taken from the dummy battery setup but the construction and experimental methods were the same as in the simulation methods. So, the results that are obtained from experiment at every different temperature are compared with the simulated results.

3.1 Free convection

3.1.1 At 46°C

Firstly, at 46°C, results were obtained and plotted in Figure 17. It shows that the reduction in temperature was greater in the simulation than in the experiment. During the experiment,

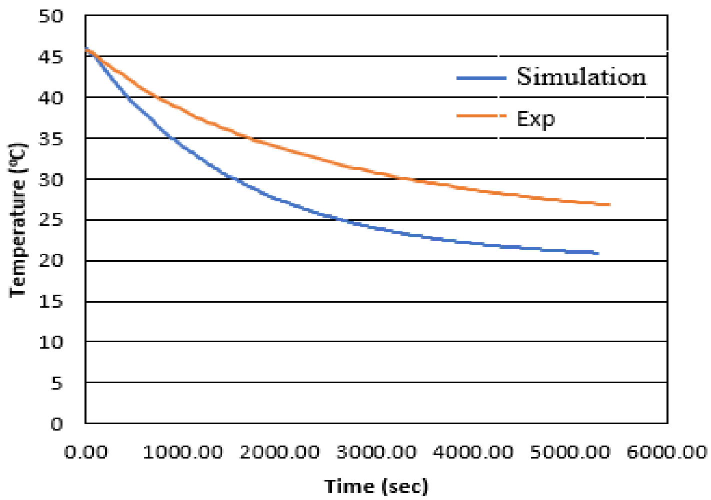

Figure 17. Comparison at 46ºC

temperature dropped from 46ºC to 26.8009ºC. However, during the simulation, temperature dropped to 20.926ºC. After 88 min of observation, the reduction in temperature was greater in the case of the simulation. There was a difference of 5ºC between the results. This was because of environmental factors that affected the results during the experiment. There was always change in ambient temperature, and it was not 20ºC for the complete time of observation. This error could be reduced by doing the experiment in a fixed temperature chamber by fixing ambient temperature as constant. The percentage of error in this result were approximately 21%.

3.1.2 At 67ºC

The results were obtained and plotted in Figure 18. During the experiment, the temperature reduced from 67ºC to 29.7576ºC. During the simulation, the temperature reduced to 21.332ºC. Across 94 min of observation, reduction in temperature was greater for the simulation. There was a difference of 8ºC between the results and it was environmental factors that affected the results during the experiment. There was always change in ambient temperature and it was not 20ºC for the complete time of observation. This error could be reduced by doing experiment in a fixed temperature chamber. The percentage of error in this result was approximately 28%.

3.1.3 At 77ºC

Thirdly, at 77ºC, the results were obtained and are plotted in Figure 19. The graph shows that the reduction in temperature was greater for the system under simulation than the system under experiment. During the experiment, the temperature reduced from 77ºC to 30.0265ºC. During the simulation, the temperature reduced to 20.796ºC. Over the full 90 min of observation, the reduction in temperature was greater for the simulation. There was a difference of 10ºC between the results. This was because of environmental factors affecting the results of the experiment. Ambient temperature varied and it was not at 20ºC over the time of observation. This kind of error could be reduced by doing experiment in a fixed temperature chamber to keep ambient temperature at constant. The percentage of error in this result was approximately 33%.

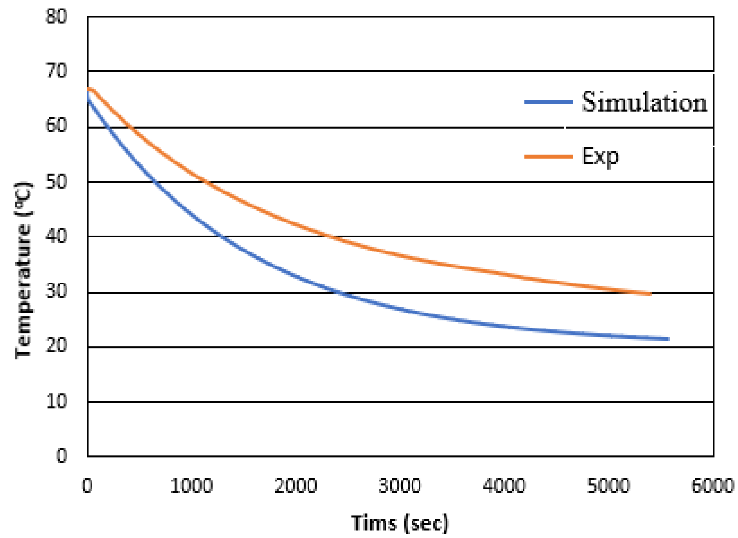

Figure 18. Comparison at 67ºC

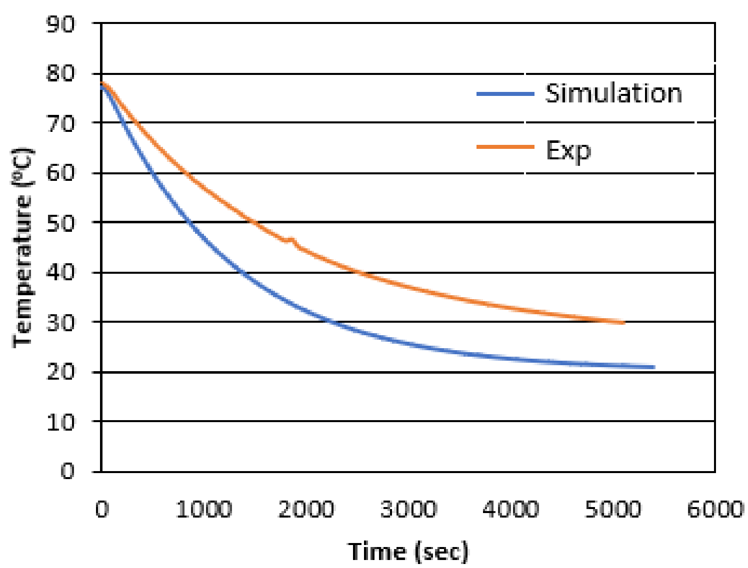

Figure 19. Comparison at 77ºC

3.2 Forced convection

3.2.1 At 67°C and 41°C

From Figure 20, the temperature reduced from 67°C to 54.067°C within 60 min. There was a reduction of 13°C. However, in the experimental result, the temperature reduced from 41.2484°C to 27.024°C within 32 min. Here, the reduction in temperature was 14°C. This difference in the experimental result was because the power input was switched off, and therefore the system was no longer heated up. That was the reason that the experimental set up cooled faster than the simulation result. Moreover, there were some additional environmental factors that affected the system under experimental observation.

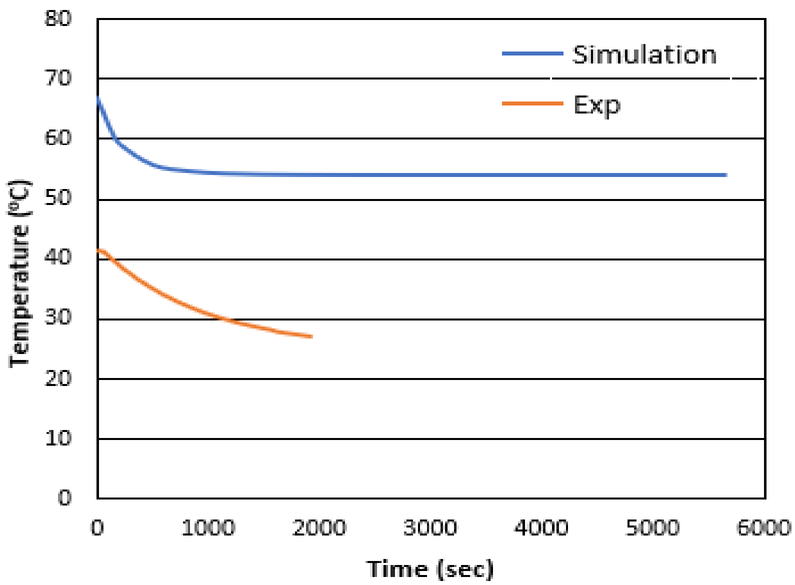

Figure 20. Comparison at 67°C and 41°C

3.2.2 At 77°C and 48°C

From Figure 21, the temperature reduced from 77°C to 67.693°C within 66 min. This was a reduction of 10°C but in experimental result, the temperature reduced from 48.1626°C to 25.6264°C within 33 min and this was a reduction in temperature of 23°C. This difference in experimental result was because the power input was switched off, and therefore the system was no longer being heated up. This was the reason that the experimental set up cooled faster than the simulation result. Moreover, there were other environmental factors that affected the system under experimental observation.

4. Conclusions

A complete battery pack with cooling set up was modeled and simulated to find the reduction in temperature. This work was carried out under the operation of free convection and forced convection using ANSYS workbench software. The main conclusions drawn are as follows.

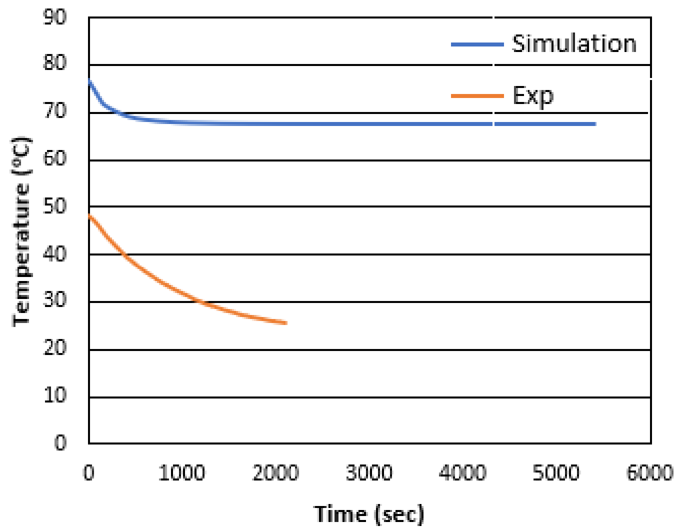

Figure 21. Comparison at 77°C and 48°C

On comparing the results, it was found that free convection on simulation was more effective than the experimental one. Also, the percentage of error varied at all the different initial temperatures. For example, at 45°C the percentage of error was 21% whereas at 67°C the percentage of error was 28%. This difference was because the ambient temperature in the experimental setup fluctuated. It was not maintained at a constant.

On the cooling system under forced convection, that is with use of an external medium like a fan or blowers to cool the system. During simulation, the temperature started to reduce from a higher temperature to the optimum temperature within a short period of time and the system kept a constant temperature. A reduction of 10°C to 20°C in temperature was achieved using an air flow at a velocity of 8.5m/s. On comparing the results of the experiments and simulation, it was concluded that battery got cooler faster during the simulation than the experiment.

Finally, it was concluded that heat reduction within the battery system was possible using a model constructed with fins made of aluminium. This system was cost effective, less complex and powerful in operation. Using this cooling method, the temperature could be maintained within its operating range thereby preventing damage to cells. Moreover, the reduction in temperature could better enhance the performance of the battery and life span of the battery.

References

[1] Zhou, H., Zhou, F., Xu, L. and Kong, J., 2019. Thermal performance of cylindrical Lithium-ion battery thermal management system based on air distribution pipe. *International Journal of Heat and Mass Transfer*, 131, 984-998.

[2] Xu, X.M., Sun, X.D., Hu, D.H., Li, R.Z. and Tang, W., 2018. Research on heat dissipation performance and flow characteristics of air-cooled battery pack. *International Journal of Energy Research*, 42(11), 3658-3671.

[3] Xie, J., Ge, Z., Zang, M. and Wang, S., 2017. Structural optimization of lithium-ion battery pack with forced air-cooling system. *Applied Thermal Engineering*, 126, 583-593.

[4] Saw, L.H., Poon, H.M., Thiam, H.S., Cai, Z., Chong, W.T., Pambudi, N.A. and King, Y.J., 2018. Novel thermal management system using mist cooling for lithium-ion battery packs. *Applied Energy*, 223, 146-158.
[5] Pang, W., Yu, H., Zhang, Y. and Yan, H., 2019. Solar photovoltaic based air-cooling system for vehicles. *Renewable Energy*, 130, 25-31.
[6] Lu, Z., Yu, X., Wei, L., Qiu, Y., Zhang, L., Meng, X. and Jin, L., 2018. Parametric study of forced air-cooling strategy for lithium-ion battery pack with staggered arrangement. *Applied Thermal Engineering*, 136, 28-40.
[7] Li, W., Xiao, M., Peng, X., Garg, A. and Gao, L., 2019. A surrogate thermal modeling and parametric optimization of battery pack with air cooling for EVs. *Applied Thermal Engineering*, 147, 90-100.
[8] Jilte, R.D. and Kumar, R., 2018. Numerical investigation on cooling performance of Li-ion battery thermal management system at high galvanostatic discharge. *Engineering Science and Technology, an International Journal*, 21(5), 957-969.
[9] Kim, J., Oh, J. and Lee, H., 2019. Review on battery thermal management system for electric vehicles. *Applied Thermal Engineering*, 149, 192-212.
[10] Chen, K., Li, Z., Chen, Y., Long, S., Hou, J., Song, M. and Wang, S., 2017. Design of parallel air-cooled battery thermal management system through numerical study. *Energies*, 10(10), 1677, https://doi.org/10.3390/en10101677.
[11] Deng, Y., Feng, C., Jiaqiang, E., Zhu, H., Chen, J., Wen, M. and Yin, H., 2018. Effects of different coolants and cooling strategies on the cooling performance of the power lithium ion battery system: A review. *Applied Thermal Engineering*, 142, 10-29.
[12] Patil, M.S., Panchal, S., Kim, N. and Lee, M.Y., 2018. Cooling performance characteristics of 20 Ah lithium-ion pouch cell with cold plates along both surfaces. *Energies*, 11(10), 2550.
[13] Chen, K., Song, M., Wei, W. and Wang, S., 2019. Design of the structure of battery pack in parallel air-cooled battery thermal management system for cooling efficiency improvement. *International Journal of Heat and Mass Transfer*, 132, 309-321.
[14] Chen, K., Chen, Y., Li, Z., Yuan, F. and Wang, S., 2018. Design of the cell spacings of battery pack in parallel air-cooled battery thermal management system. *International Journal of Heat and Mass Transfer*, 127, 393-401.
[15] Wang, Y., Moura, S.J., Advani, S.G. and Prasad, A.K., 2019. Power management system for a fuel cell/battery hybrid vehicle incorporating fuel cell and battery degradation. *International Journal of Hydrogen Energy*, 44(16), 8479-8492.
[16] Al-Zareer, M., Dincer, I. and Rosen, M.A., 2019. A novel approach for performance improvement of liquid to vapor based battery cooling systems. *Energy Conversion and Management*, 187, 191-204.
[17] Jiaqiang, E., Yue, M., Chen, J., Zhu, H., Deng, Y., Zhu, Y., Zhang, F., Wen, M., Zhang, B. and Kang, S., 2018. Effects of the different air-cooling strategies on cooling performance of a lithium-ion battery module with baffle. *Applied Thermal Engineering*, 144, 231-241.
[18] Bai, F.F., Chen, M.B., Song, W.J., Li, Y., Feng, Z.P. and Li, Y., 2019. Thermal performance of pouch Lithium-ion battery module cooled by phase change materials. *Energy Procedia*, 158, 3682-3689.
[19] Nimmagadda, R., Reuven, R., Asirvatham, L.G. and Wongwises, S., 2020. Thermal management of electronic devices using gold and carbon nanofluids in a lid-driven square cavity under the effect of variety of magnetic fields. *IEEE Transactions on Components, Packaging and Manufacturing Technology*, 10(11), 1868-1878.
[20] Nimmagadda, R., Matta, D.P., Reuven, R., Asirvatham, L.G., Wongwises, S., Yerramilli, A. and Adusumilli, S., 2020. Effect of magnetic field on the laminar heat transfer performance of hybrid nanofluid in a lid driven cavity over solid block. *Proceedings* of *ASME Power Conference*, Virtual, Online, August 4-5, 2020, pp. 1-9.

[21] Nimmagadda, R. and Venkatasubbaiah, K., 2015. Multiphase approach on heat transfer performance of micro-channel using hybrid carbon nanofluid. *Proceedings of International Conference on Nanochannels, Microchannels, and Minichannels*, San Francisco, USA, July 6-9, 2015, pp. 1-9.

[22] Rao, G.S., Rao, G.K. and Raju, S.S.N., 2014. An innovative approach to battery management and propulsion system of electric/hybrid electric vehicle. *International Journal of Electric and Hybrid Vehicles*, 6(1), 1-13.

[23] Panjagala, H., Madhukar, E.L.N.R. and Kiran, I.R., 2018. Recent advancements in shape optimization of aero spiked high-speed re-entry vehicle using CFD. *MATEC Web of Conferences*, 172, https://doi.org/10.1051/matecconf/201817201007.

[24] Babu, S.S. and Yasin, S., 2019. Heat transfer analysis of automobile radiator with helical tubes using CFD. *International Journal of Innovative Technology and Exploring Engineering*, 8(8), 999-1003.

[25] Murali, G., Nagavamsi, V., Srinath, A. and Prakash, M.A., 2020. Battery thermal management system using phase change material on trapezoidal battery pack with liquid cooling system. *International Journal of Advanced Science and Technology*, 29(5), 5288-5300.

[26] Returi, M.C., Konijeti, R. and Dasore, A., 2019. Heat transfer enhancement using hybrid nanofluids in spiral plate heat exchangers. *Heat Transfer-Asian Research*, 48(7), 3128-3143.

[27] Srilatha, A., Pandian, A. and Varma, P.S., 2020. Multilevel charging of lithium-ion battery for fast charging stations of EV's. *International Journal of Advanced Science and Technology*, 29(4), 858-871.

[28] Murali, G., Nagendra, B. and Jaya, J., 2020. CFD analysis on heat transfer and pressure drop characteristics of turbulent flow in a tube fitted with trapezoidal-cut twisted tape insert using Fe_3O_4 nano fluid. *Materials Today: Proceedings*, 21, 313-319.

[29] Rao, K.N. and Radha, G.V.G., 2020. Comparative study by numerical investigation of heat transfer in circular tube by using hybrid nanofluids. *International Journal of Mechanical and Production Engineering Research and Development*, 10(3), 969-982.